General Search Results--Full Record

Article 2 of 2
MARK
Explanation

A STUDY OF ATMOSPHERIC DIFFUSION FROM THE LANDSAT IMAGERY
VISWANADHAM Y, **TORSANI JA**
JOURNAL OF GEOPHYSICAL RESEARCH-OCEANS AND ATMOSPHERES
87 (NC12): 9621-9635 1982

Document type: Article **Language:** English **Cited References:** 59 **Times Cited:** 3

Addresses:
VISWANADHAM Y, CONSELHO NACL DESENVOLVIMENTO CIENT & TECNOL,INST PESQUISAS ESPACIAIS,SAO PAULO,BRAZIL

Publisher:
AMER GEOPHYSICAL UNION, WASHINGTON

IDS Number:
PS781

ISSN:
0148-0227

Article 2 of 2

JOURNAL OF GEOPHYSICAL RESEARCH, VOL. 87, NO. C12, PAGES 9621-9635, NOVEMBER 20, 1982

A STUDY OF ATMOSPHERIC DIFFUSION FROM THE LANDSAT IMAGERY

Y. Viswanadham and J. A. Torsani

Instituto de Pesquisas Espaciais - INPE
Conselho Nacional de Desenvolvimento Científico e Tecnológico - CNPq, São Paulo, Brazil

Abstract. Detailed analyses of the LANDSAT multispectral scanner (MSS) data of the smoke plumes that originated in eastern Cabo Frio (22° 59'S; 42° 02'W) and crossed over into the Atlantic ocean are presented to illustrate how high-resolution LANDSAT imagery can aid meteorologists in evaluating specific air pollution events. The eleven LANDSAT images selected are for different months and years. Conventional interpretation techniques are applied to analyze the images with a view to arrive at certain plume characteristics. The analysis of the visible smoke plumes revealed that the plume was 130 km long and attained a maximum width of 937 m, 10 km away from the chimney emitting the effluent. The results show that diffusion is governed primarily by water and air temperature differences. With colder water, low-level air is very stable and the vertical diffusion is minimal; but water warmer than the air induces vigorous diffusion. The applicability of two empirical methods for determining the horizontal eddy diffusivity coefficient (K_y) in the Gaussian plume formula was evaluated with the estimated standard deviation of the crosswind distribution of material in the plume (σ_y) from the LANDSAT imagery. Most consistent estimates for K_y are obtained from the formula based on Taylor's theory of 'diffusion by continuous moment.' K_y values of about 158 $m^2 s^{-1}$ in quasi-neutral conditions and 49 $m^2 s^{-1}$ in stable conditions are obtained from a plot of σ_y^2 as a function of distance from the source. The rate of kinetic energy dissipation (ε) is evaluated from the diffusion parameters σ_y and K_y. The ε value ranges from 0.1×10^{-5} $m^2 s^{-3}$ to 80.2×10^{-5} $m^2 s^{-3}$ in quasi-neutral and stable stratifications. These results compare well with the previous experimental values obtained over water surfaces by various workers. They form a data base for use in the development and validation of mesoscale atmospheric diffusion models.

1. Introduction

Increased concern for the environmental effects of power plants located on coastal sites and plants proposed for sites offshore has created a need for improved methods to estimate atmospheric diffusion rates over open water. (The more or less interchangeable use of the terms 'diffusion' and 'dispersion' is intended to convey the idea that the smoke particles in this study are regarded as having ideal, nondynamical, fluid attached properties [Gifford, 1957].) The diffusion properties of the coastal marine atmosphere are unique, principally because the air flows over significantly smoother surfaces, and these conditions have been studied far less than flows over land. That is not to say that the marine boundary layer has not been explored. Because of the difficulty in measuring the instantaneous values of concentration simultaneously at a sufficient number of positions, the observation of relative diffusion has tended to rely mainly on the visual methods, and especially on the observation of the growth and dissipation of puffs of smoke. Earliest examples are contained in discussions of Roberts [1923] and Sutton [1932], in which photographic observations of the growth of antiaircraft shell bursts were used to test theoretical treatments. Later and more extensive series of observations of this type have been reported by Kellogg [1956], and Frenkiel and Katz [1956].

A comprehensive survey of earlier dispersion experiments conducted over oceans and shorelines reported by Prophet [1961] discusses the changing characteristics of flows passing from land to water; a subsequent review by Van der Hoven [1967] summarizes atmospheric dispersion studies conducted during onshore winds and classifies various flow regimes as overwater, overland, or in transition from water to land. Perhaps because of the difficulties encountered in conducting meteorological experiments over water, relatively few such studies have been made. Slade [1962] measured air-water temperature differences, mean wind speeds, and wind direction fluctuations on the upwind and downwind shores of Chesapeake Bay to obtain estimates of the relative intensities of atmospheric turbulence over land and water. Also, studies of coastal meteorology and diffusion were summarized by Raynor et al. [1975, 1978].

Techniques of utilizing smoke-plume photographs to obtain quantitative estimates of diffusion were first proposed by Richardson [1920] and Roberts [1923], and afterwards applied by Holland [1953], Browne [1961], Culkowski [1961], and Högström [1964]. Whitehead et al. [1969] showed that cloud photographs taken during the Apollo 6 mission offered significant meteorological information because of their excellent detail and their adaptability to relative height contouring by stereographic photogrammetry. McLellan [1971] was among the first to attempt to use satellite data to measure anthropogenic pollution by examining the digital brightness values in ATS visible data over the Los Angeles basin. During the Apollo 6 mission, Randerson et al. [1971] have acquired a number of color photographs containing a smoke plume. An earlier analysis of such plumes, utilizing earth satellite photography, was also undertaken by Randerson [1968] who demonstrated

Paper number 2C0985.
0148-0227/82/002C-0985$05.00

that satellite photography could be utilized to study the large-scale transport of atmospheric pollutants.

Lyons and Pease [1973] have presented a series of LANDSAT 1 satellite images showing that, indeed, smoke plumes from the industrial complex around Chicago - Gary travelled for long distances over water. Lyons [1975a, b] explained that the high-resolution multispectral LANDSAT 1 image usually will only detect smoke plumes over water surfaces. Griggs [1973] and Mekler et al. [1977] have suggested using LANDSAT radiance measurements in the visible bands to infer aerosol optical thicknesses and, therefore, the columnar aerosol density over low albedo (water) surfaces. While the technique shows great promise, the LANDSAT images are made over any given region on the earth only every 9 or 18 days in a narrow strip 180 km wide and thus do not make it a likely candidate for an operational monitoring system.

The aim of the present study is to find some clues to the problems of diffusion over ocean by using LANDSAT imagery. The cases illustrated here may be considered typical of the diffusion from a continuous point source and the simplest kind of pollution over ocean. They illustrate how satellite data have furthered our knowledge of long-range transport and indicate the feasibility of estimating the lateral standard deviation, the dissipation rate and the diffusion coefficients of smoke plume from spacecraft.

2. Theoretical Considerations

As an introduction to the working formulae, it is useful to consider certain convenient procedures. Consider idealized cases of instantaneous and continuous sources in a homogeneous air stream, with the x axis in the direction of the mean wind, supposed horizontal, the y axis across wind and the z axis vertical. The mean wind is assumed to be constant in space, while the mean components of velocity in the crosswind and vertical directions are zero. Ideally it is assumed that the instantaneously generated cloud moves in a straight line parallel to the x axis, expanding in all directions, while the fixed continuous source generates a symmetric plume around the fixed x axis, with an expanding cross section in the y, z plane. The practical sucess of explicit diffusion formulae thus depends on the extent to which correct choices of the distribution shape, the lateral standard deviation σ_y, and the vertical standard deviation σ_z are contained therein. Comparison with the observations then enable the correctness of the original diffusion treatment to be assessed, and parameters such as diffusion coefficients and intensities of turbulence to be evaluated

Single-particle diffusion addresses the problem location of a single particle released from a fixed point. The theoretical foundation was laid down by Taylor [1921] in his historic paper, 'Diffusion by Continuous Movement.' Relative diffusion concerns the position of two particles released from a single point relative to their mutual center of gravity. The major contribution to the theory of relative diffusion is that of Batchelor [1949, 1952], although Richardson [1926] acknowledged the problem many years earlier. The apparent lateral eddy diffusivity coefficient (K_y) is defined as

$$K_y = \frac{1}{2} \frac{d\sigma_y^2}{dt} \tag{1}$$

where t is the time. This relationship between the apparent K_y and σ_y along the y axis was derived by Batchelor [1949]. Unlike Fickian diffusion, the scale of plume need not be larger than the scale of turbulence since the K_y in (1) depends on the standard deviation $\sigma_y(t)$, which according to Taylor's [1921] theorem, depends on the entire energy spectrum. By virtue of Taylor's hypothesis, (1) becomes

$$K_y = \frac{1}{2} \bar{u} \frac{d\sigma_y^2}{dx} \tag{2}$$

where $\bar{u}$ is the mean wind speed along the x axis. Here, it is assumed that Taylor's hypothesis is applicable to the flow with homogeneous turbulence in the lateral at each horizontal plane. For steady state flow, it is no longer necessary to assume the validity of Taylor's hypothesis, and the apparent K_y is defined as in (2). The apparent K_y depends on the height and the downwind distance; the increase of the lateral mixing with height is due to the increase in the size of eddies, as particles are displaced further away from the boundary. As a consequence of using the apparent K_y, the predicted concentration distribution in the crosswind direction is of Gaussian distribution. This result is consistent with the application of the statistical theory used in the derivation of the Gaussian diffusion model.

Incidentally, the dissipation rate of turbulent energy ϵ is estimated. Many studies on the turbulent diffusion have been carried out since Richardson [1926], and the following is familiar:

$$K_y \propto \epsilon^{1/3} \sigma_y^{4/3} \tag{3}$$

where σ_y is the scale of the diffusion process. This 4/3 power relation is that derived from Heisenberg's [1948a, b] treatment of eddy viscosity and, as found by Richardson, applies over a very wide range of σ_y, much wider in fact than would be expected from the similarity hypotheses and the ideas about the isotropy of the atmospheric turbulence. It may be, however, that very large atmospheric eddies, which certainly are not isotropic (their vertical motions are necessarily small compared with their horizontal motions), tend to a state of restricted isotropy, in the horizontal.

The Gaussian diffusion model has made a significant contribution to diffusion estimates. Gifford [1959, 1968] generalized the Gaussian diffusion model to several simple formulas specially adapted to yield diffusion coefficients directly from photographic measurements of average plume dimensions. Of particular interest in this case are the following two equations for evaluating the lateral eddy diffusivity coefficient K_y:

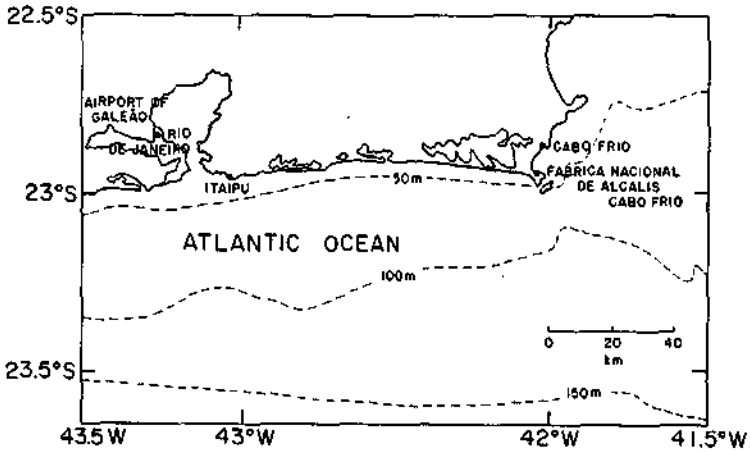

Fig. 1. Map of a portion of the Brazilian coastal area showing Cabo Frio region, Fábrica Nacional de Alcalis and Airport of Galeão. Ocean depth contour lines in 50-m intervals.

$$K_y = \frac{\bar{u}\, Y_m^2 \exp(1/3)}{2X_t} \qquad (4)$$

$$K_y = \frac{\bar{u}\, Y_m^2}{2\, X_m} \qquad (5)$$

where X_t is the total plume length and X_m is the distance downwind from the source at which the maximum plume width Y_m occurs.

3. Site and Weather Conditions

Fábrica Nacional de Alcalis (National Chemicals Industry) is located on the east shore of Cabo Frio, about 120 km east of Rio de Janeiro city in the state of Rio de Janeiro, Brazil (Figure 1). The Cabo Frio area (22° 59'S; 42° 02'W) of eastern Brazil is a flat coastal region bounded north-west by land and the rest by Atlantic ocean. The coast is straight, uncomplicated and typical of much of the northern and southern seaboard from Cabo Frio town. East of Itaipu the ocean is separated from the mainland by a low barrier beach and shallow lacks; water depths increase gradually to about 50 m at 5 km from the shore, approximately.

Fábrica Nacional de Alcalis is 7 m above mean sea level. The Cabo Frio region has a tropical temperature regime with a mean annual temperature 20°C and an average rainfall of 1600 mm [WMO, 1975]. Particularly during spring and summer months, sea breezes occur on a large percentage of all days in the afternoon, approximately 1200 to 1700 hours local time. During this period, winds are relatively strong throughout the area. The mean monthly atmospheric mixing heights vary between 870 and 1220 m [Nicolli, 1977].

Weather in the region is subject to variations of the position of the tropical maritime anticyclone with easterly winds blowing on the coast. The cold polar anticyclone in Argentina, by its presence, pushes the tropical maritime high, and the winds back to northeast, north, and finally northwest on the approach of the cold front. Then the winds change back to southwest, southeast, as the cold front advances northeastward. This cycle repeats itself as the cold polar anticyclone, already in low latitudes, degenerates into the tropical maritime anticyclone. From July to December the cycle is quick and slows down from January to June since the cold air mass is not strong enough to push the tropical anticyclone into the ocean. The effect is a seasonal one with a dominance of easterlies or northeasterlies during summer and fall, and southwesterlies or westerlies during winter and spring. The Cabo Frio region is noted for its upwelling, which has a great biological importance in the production and variation of fish 'Sardinella aurita' [Silva, 1971].

4. Data Sets and Processing

4.1. Emission Parameters and Meteorological Data

The visible smoke plumes obtained from the LANDSAT imagery are emitted by the Fábrica Nacional de Alcalis of Brazil. The emission parameters from the 76-m stack height of the industry are gas flow rate (200 $m^3\ s^{-1}$), exit gas speed (7 $m\ s^{-1}$), and gas composition by volume (47% of water vapor, 41% of N_2, 10% of O_2, 2% of CO_2 and traces of CO, NO_x, SO_2, Mg, $MgSO_4$, and NaCl) (Companhia Nacional de Alcalis, personal communication, 1981).

The meteorology of urban coastal regions generally differs considerably from the features of inland urban areas. The mesoscale meteorological conditions existing during the period (1975-1978) of interest could be approximated from available data of two agencies. Owing to the lack of adequate meteorological measurements for inland and oceanic areas of the Cabo Frio region at the time of LANDSAT imagery, the upper air observations data were taken from the international airport of Galeão, Rio de Janeiro, Brazil [Força Aérea Brasileira, 1974-1978]. Surface weather conditions, i.e., wind speed and prominent wind direction at 10-m

TABLE 1. Reference Number of LANDSAT Image Cases (n) and Various Meteorological Parameters

n	Date	Time in Hours		C	Wind Speed, m s^{-1}		DDD	Temperature, °C		$\frac{\partial\theta}{\partial z}$	Inversion Height, m		RI
		GMT	Local		10 m	76 m		T_s	T_h	°K/100 m	Base	Top	
1	April 18, 1975	1157	0857	20	1.0	4.8	N	25.0	24.4	- 0.72	1600	2000	- 0.071
2	Dec. 8, 1975	1144	0844	40	(-)	4.6	NE	25.0	24.5	- 0.70	-	-	- 0.065
3	Feb. 18, 1976	1139	0839	50	5.8	1.6	NNE	27.0	26.8	- 0.16	-	-	- 0.013
4	March 7, 1976	1138	0838	10	(-)	6.4	NE	26.0	25.5	- 0.61	-	-	- 0.028
5	June 23, 1976	1130	0830	0	8.3	4.1	NNE	23.0	23.5	0.56	1300	1500	0.046
6	Feb. 3, 1977	1150	0850	10	7.1	10.7	NE	26.0	25.4	- 0.77	-	-	- 0.085
7	March 11, 1977	1153	0853	10	4.1	8.0	NE	28.0	28.2	0.06	Surface	400	0.006
8	May 22, 1977	1145	0845	40	1.1	4.0	W	21.0	21.5	0.47	Surface 1800	900 2500	0.081
9	June 9, 1977	1144	0844	0	(-)	3.3	W	22.0	21.5	- 0.60	-	-	- 0.106
10	Oct. 31, 1977	1136	0836	20	10.0	5.0	NNE	26.0	26.6	0.70	Surface	400	0.040
11	July 1, 1978	1205	0905	0	2.5	4.6	N	23.0	23.2	0.27	Surface	500	0.088

C is the cloud cover in percent, DDD is the prominent wind direction, T_s is the screen temperature, T_h = 76-m stack height temperature, $\partial\theta/\partial z$ is the potential temperature gradient below 80 m, and RI is the Richardson gradient number. Dashes indicate missing data. The wind speed at 76-m stack height level, T_h and $\partial\theta/\partial z$, are obtained from radiosonde ascents at the international airport of Galeão. The stability parameter RI is calculated by using mean value of T_s and T_h and the wind shear between 10 and 76 m. In the case of missing wind data at 10-m level, the wind shear is obtained after dividing the 76-m level wind speed by 76 m.

height, screen dry-and wet-bulb temperatures, solar insolation and cloud cover for 6-hour intervals starting from midnight are available at a weather station [Instituto Nacional de Meteorologia, 1968-1978] very close to the industry. The radiosonde soundings for each LANDSAT imagery were plotted for the three-day period (one day before and one day after the passage of satellite) along with the surface data. Then, the interpolated mean wind speed was obtained at 76-m stack height level. In Table 1, the base and top of the inversion heights are presented along with other details.

4.2. Satellite Data

The application of LANDSAT imagery in the earth sciences is steadily gaining favor. It is particularly useful for the study of areas where accurate ground truth is difficut to obtain. The Instituto de Pesquisas Espaciais (INPE), Brazil, has issued maps with path and row number of the area over which they can receive LANDSAT satellite multispectral scanning (MSS) data in real time. The classification of the four channel low-resolution scene was carried out on an interactive display system GE - Image 100 [General Electric Company, 1975]. The primary function of the Image 100 system is to extract thematic information from multispectral imagery. A secondary function is as an image enhancement system. Using this system, LANDSAT/MSS data were processed digitally to perform image rectification and classification. In order to derive accuracy information, a verification procedure based upon a systematic random sampling scheme was applied to the digitally processed classification LANDSAT and terrain data sets. Examples of processed imagery are presented in section 4 of General Electric Company [1974] in order to illustrate practical application of Image 100.

Eleven LANDSAT images of the Cabo Frio region were obtained at an average local time between 0830 to 0930 hours, with a view to arrive at certain smoke plume characteristics. They were selected for analysis on the basis of having a minimum of fair data quality in bands 4, 5, 6 and 7, and no interference from clouds over the study site (Table 1). The thematically classified LANDSAT data produced by digitizing 1:100,000 scale maps appear to be suitable for portraying elevations for the present study. The images selected on the basis of acceptable quality were found to coincide with the local time of radiosonde ascents at Galeão Airport, approximately.

Computer compatible tapes and interactive multispectral analysis systems allow individual picture elements to be analyzed and displayed by using statistical and mathematical processing functions. The enhanced images were displayed in the video equipment and photographed with Kodak color II - 100 ASA - 35 mm negative film and also with Ektachrome - 64 ASA - 35 mm slide film. The photographed films were used for subsequent enlargement to the size of 45.5 x 70.0 cm on a transparent paper (Figure 2), and measurements were made of the plume dimensions with the aid of a 3 M Brand, 201 Dry Silver Reader Printer.

The crosswind dimension of a smoke plume is conventionally represented by the width between positions at which concentration falls to a given fraction (usually one-tenth) of the central value (Figure 2). When the distribution is of Gaussian form and the fraction adopted in specifying smoke plume width ($2\,Y_0$) is one-tenth, the standard deviation of the crosswind displacement of the material σ_y, in practice defined by Pasquill [1961] and Gifford [1961], is

$$\sigma_y = 2\,Y_0/4.3 \qquad (6)$$

Estimates of σ_y were obtained from measurements of visible plume width on all usable photographs with known geometric relationship (6). These

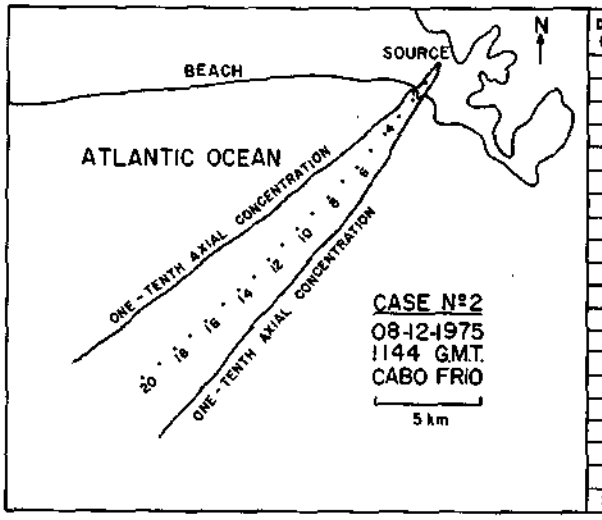

DIST (km)	2Yo (m)	σ_y (m)
1	417	97
2	583	136
3	833	194
4	1166	271
5	1417	329
6	1667	387
7	2000	465
8	2250	523
9	2500	581
10	2666	620
11	2924	680
12	3182	740
13	3483	810
14	3741	870
15	4000	930
16	4214	980
17	4515	1050
18	4730	1100
19	4988	1160
20	5246	1220

Fig. 2. Evaluation of σ_y from the LANDSAT image of 1144 GMT December 8, 1975, for the Cabo Frio region.

smoke plume spread measurements can be converted into useful information regarding over-water mesoscale diffusion of pollutants.

5. Results

5.1. General Observations of Plume Behavior

The foregoing classification of smoke plumes from LANDSAT imagery provides a useful approach to the broad specification of diffusion in terms of general weather conditions. They may be used in assessing the quality of diffusion effects on particular occasions. However, apart from the qualitative nature of the results, there are numbers of limitations in the present approach due to the meteorological data sets, topography and climatology of the site. For the achievement of quantitative and reliable estimates of diffusion it is necessary to have accurate simultaneous turbulence measurements in space and time. To be exact, the characteristic variation of wind structure with height above ground should be taken into account. But the over-all effect of mesoscale motions would most likely be an increased diffusion over water. In Table 1, reference number of LANDSAT image cases, various meteorological parameters, heights of inversion base and top, and the gradient Richardson number are presented for a qualitative description of the smoke plumes. A deep surface super-adiabatic layer failed to form, however, due to the relatively weak sunshine. The Richardson gradient numbers that were computed by taking temperature differences below the 80-m level of the radiosonde show that quasi-neutral and stable conditions predominated. The radiosonde data did detect surface inversions below 900 m and also elevated ones beginning about 1300 m, extending to about 2500 m, in some cases (Table 1).

Figures 3-13 are portions of the LANDSAT images taken at approximately 1130 to 1205 GMT during the period April 1975 to July 1978 for the Cabo Frio region. These figures illustrate typical phenomena that occur in a coastal transition zone during a period of quasi-neutral and stable offshore air flow over a water surface. Mixing depths over the water are greatly restricted and turbulence values are

Fig. 3. An April 18, 1975, LANDSAT image at 1157 GMT of smoke plume of the Cabo Frio region drifting northeastward across the Atlantic Ocean. It has an initial portion that is 50 km long, and associated with a horizontal wind speed, $u = 4.8\ m\ s^{-1}$, and a vertical temperature gradient, $(\partial\theta/\partial z) = -7.20^{\circ}K\ km^{-1}$. There is a discontinuity of the plume approximately at about 15-km distance from the source. Image photographically enhanced from original 35-mm slide.

Fig. 4. As in Figure 3 except for 1144 GMT December 8, 1975. The plume has an initial portion that is 40 km long and is associated with $u = 4.6$ m s^{-1} and $(\partial\theta/\partial z) = -7.00^{\circ}K\ km^{-1}$. There were no clouds present in this view, only turbid and hazy conditions owing to upwelling in this period.

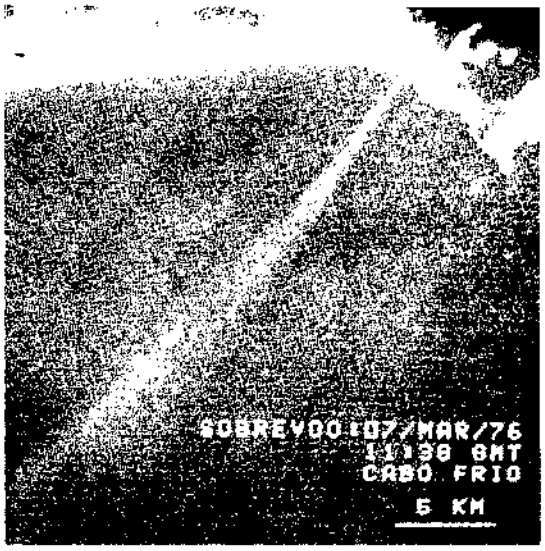

Fig. 6. As in Figure 3 except for 1138 GMT March 7, 1976. The air was so slightly unstable that the plume could be seen extending for 120 km with $u = 6.4$ m s^{-1} and $(\partial\theta/\partial z) = -6.10^{\circ}K\ km^{-1}$. It is a well defined plume with marked boundaries.

small. If one compares the slopes of the plume axes on different traverses, one can see a great deal of variance. For much of the days the plumes appeared approximately in NNE direction.

The prime cause for such variations is the directional shear of the wind, which can be a rapidly changing parameter [Högström, 1964; Smith, 1965]. In most of the cases, the winds oscillated very little at 80-m altitudes, and

Fig. 5. As in Figure 3 except for 1139 GMT February 18, 1976. The plume has an initial portion that is 40 km long and is associated with $u = 1.6$ m s^{-1} and $(\partial\theta/\partial z) = -1.60^{\circ}K\ km^{-1}$. It has a concave nature approximately between 10-and 18-km distances from the source. Cumulus clouds are visible on the left side of the photo.

Fig. 7. As in Figure 3 except for 1130 GMT June 23, 1976. The air was so stable that the plume could be seen extending for 130 km with $u = 4.1$ m s^{-1} and $(\partial\theta/\partial z) = 5.60^{\circ}K\ km^{-1}$. But, over water fetch the air temperature was slightly colder than the ocean surface temperature. The formation of cumulus cloud streets are visible over the ocean in the right side of the photo.

Fig. 8. As in Figure 3 except for 1150 GMT February 3, 1977. The plume is not a well defined one. It is exhibiting mixing in the shallow turbulent layer above the ocean. It has an initial portion that is 40 km long and is associated with a high value of $u = 10.7$ m s^{-1} and $(\partial\theta/\partial z) = -7.70^{\circ}K\ km^{-1}$. Image quality is severely degraded by rephotography.

Fig. 10. As in Figure 3 except for 1145 GMT May 22, 1977. The plume has more than 20 km long in length. It is drifting southwestward with $u = 4.0$ m s^{-1} and $(\partial\theta/\partial z) = 4.70^{\circ}K\ km^{-1}$. Water temperature is slightly greater than air temperature, but the radiosonde ascent showed the surface and higher level inversions. The plume is exhibiting mixing and undefined boundary contours.

Fig. 9. As in Figure 3 except for 1153 GMT March 11, 1977. The plume is not a well defined one. In this case the water temperature is slightly colder than air temperature. It has an initial portion that is 100 km long and is associated with $u = 8.0$ m s^{-1} and $(\partial\theta/\partial z) = 0.60$ $^{\circ}K\ km^{-1}$. It can be seen that the conditions of the atmosphere were hazy and granular.

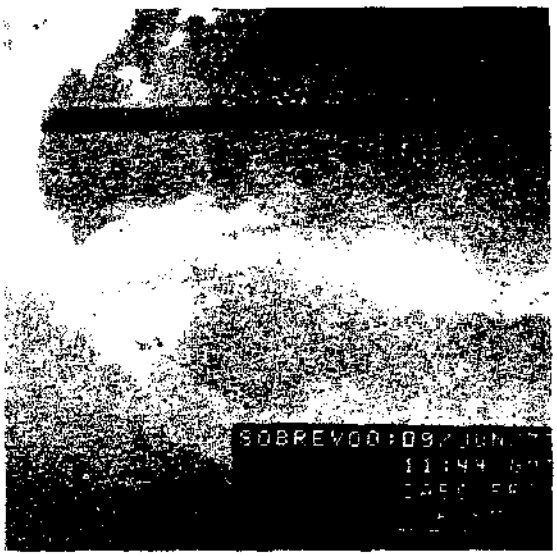

Fig. 11. As in Figure 3 except for 1144 GMT June 9, 1977. The plume has more than 30 km long in length. It is drifting southwestward and westward with $u = 3.3$ m s^{-1} and $(\partial\theta/\partial z) = -6.00$ $^{\circ}K\ km^{-1}$. The ocean surface temperature is greater than air temperature. It is exhibiting undefined contour pattern in a turbid and hazy atmosphere.

Fig. 12. As in Figure 3 except for 1136 GMT October 31, 1977. The air was so stable that the plume could be seen extending for 80 km with $u = 5.0$ m s^{-1} and $(\partial\theta/\partial z) = 7.00^{\circ}$K km^{-1}. Image quality is degraded by rephotography.

there was comparatively a small variation of directional shear. Wind speeds at plume levels approached approximately 2 to 11 m s^{-1} during the late morning, but gradually diminished to less than 4 m s^{-1} by late afternoon. From Figures 3-13, one gets the distinct impression that the turbulent plume rising from the stack is being literally blown over in response to

Fig. 13. As in Figure 3 except for 1205 GMT July 1, 1978. The air was so stable that the plume could be seen extending for 130 km with $u = 4.6$ m s^{-1} and $(\partial\theta/\partial z) = 2.70^{\circ}$K km^{-1}. A strong clockwise surface water current is visible on the right side of the island.

increasing wind speed. Also, plume trapping is a common diffusion penomenon that occurs over land, water in transitional zones, such as coastlines.

Saffman [1962] and Csanady [1969] have developed theories for diffusion from an instantaneous point source in winds exhibiting speed and directional shear. Csanady [1972] found that the lateral spread of a pollutant plume may be dominated by directional shear when the pollutant has mixed sufficiently within the shear layer. In general, the present results (Figures 3-13) agree in their general features with those obtained in the theoretical studies by Saffman [1962], Högström [1964], Smith [1965], and Csanady [1969], and in a numerical study by Tyldesley and Wallington [1965].

An important consideration is the choice of the appropriate LANDSAT spectral band to provide optimum discrimination of a particular plume against the underlying surface, in this case water. Lyons and Pease [1973] have presented a critical discussion about the combined effects of high water spectral albedo and low inherent image contrast. They have also presented other theoretical considerations regarding the poorest plume discrimination above a water surface. The plume will be most visible on the photograph when the difference between the optical density of the plume image and the optical density of the ocean-surface image is greatest (e.g., Figures 3, 5, 6, 7, and 13). A consequence of the greater transparency of water in the blue and green portion of the spectrum occurs in the case of shallow water, where reflection from the deep ocean layers may further increase the value of the ocean surface albedo and limit the ability to detect pollution plumes (e.g., Figures 8, 9, and 12). It should be noted that due to the various degradations involved both in making the photographic print and in publication, the plumes (Figures 8, 9, and 12) do not appear as clearly as they do in the original 35-mm negatives.

Further complications arise when the assumptions of 'steady state' plumes are employed. Rapid variations in wind vectors with space and time are characteristic of the coastal environment. Not only does the specification of diffusion become difficult, but pollutant transport (as determined by the orientation of the plume center line) is found to be exceedingly complex. For better interpretation of Figures 3-13, we could not find any meaningful meteorological surface and upper air data over the ocean except the data sets summarized in Table 1. Satellite measurements of water temperature are not routinely distributed. Ship reports are too sporadic and difficult to obtain. In dealing with Figures 3-13, it will clearly be necessary as a minimum to have measurements or estimates of horizontal plume meander, as well as the usual quantities required to define the turbulent type. Thus, a critical interpretation of Figures 3-13 is restricted in their nature. To present considerable discussion of results and to compare favorably with previous studies, the LANDSAT images (Figures 3-13) are grouped into two categories: (1) short plumes (i.e., $X_t < 80$ km) and (2) long plumes (i.e., $X_t \geq 80$ km).

TABLE 2. Estimated Lateral Standard Deviation σ_y (m) and Lateral Eddy Diffusivity Coefficient K_y (m^2 s^{-1}) from LANDSAT Images

n	RI	$\bar{u}$, $m\,s^{-1}$		Distance From Source in km										Mean
				1		5		10		15		20		
1	- 0.071	4.8	σ_y	100		260		520		-		-		293
			K_y		11		117		-		-			64
2	- 0.065	4.6	σ_y	97		329		620		930		1220		639
			K_y		57		127		221		287			173
3	- 0.013	1.6	σ_y	80		160		341		601		862		409
			K_y		4		15		39		61			30
4	- 0.028	6.4	σ_y	80		220		421		621		782		425
			K_y		34		82		133		247			124
5	0.046	4.1	σ_y	72		136		218		309		454		238
			K_y		7		12		20		45			21
6	- 0.085	10.7	σ_y	70		270		600		-		-		313
			K_y		91		307		-		-			199
7	0.006	8.0	σ_y	116		552		800		988		1162		724
			K_y		291		268		269		299			282
8	0.081	4.0	σ_y	80		401		-		-		-		241
			K_y		62		-		-		-			62
9	- 0.106	3.3	σ_y	116		543		601		698		891		570
			K_y		116		22		42		101			70
10	0.040	5.0	σ_y	79		224		469		612		734		424
			K_y		22		85		77		82			67
11	0.088	4.6	σ_y	84		169		258		328		412		250
			K_y		12		17		19		29			19

$\bar{u}$ is the mean wind speed at 76-m stack height level. K_y is calculated from (2)

5.2 Short Plumes

Now, we will examine the cases of short plumes (Figures 3, 4, 5, 8, 10, and 11) over marine atmosphere. In all these cases the ocean region was largely cloud free. Except two cases (Figures 10 and 11), the other plumes emitted into marine air show limited vertical diffusion. Raynor et al. [1975] have presented one unstable short plume from a boat stationed offshore during periods of onshore flow. The present study, though admittedly preliminary, suggests some obvious results of Raynor et al. [1975].

Figures 3, 4, 5, and 8 show that the turbulent intensities over water surfaces frequently appear to be lower than over land [Slade, 1962; Van der Hoven, 1967] because of (1) reduced aerodynamic surface roughness, and (2) buoyancy forces resulting from air mass stabilization during periods of warm air advection over colder waters. Thus, both the mechanical and thermal components of turbulence can be affected and diffusion rates diminished. On the other hand, during periods of advection of colder and/or drier air over water, active thermal convection patterns can generate intense turbulence on several scales (see cumulus clouds on the left side of Figure 5). Furthermore, since moist air is lighter than dry air at the same dry bulb temperature, during periods of significant evaporation buoyant forces can also be more intense than equivalent conditions over land. These buoyancy forces over evaporating surfaces have been considered in a variety of studies [e.g., LeMone, 1980].

Figure 3 shows a break-up in the plume. This is related to wind shifts in the marine boundary layer. From Figures 3, 4, 5, and 8, it must be noticed that as long as the air over the ocean is warmer than the underlying water surface, no penetrative convection will occur during the many hours of cross-ocean flow. Also, skies were clear. Thus the layers above 76 m (where the stack plumes reside) did not show as marked a difference in plume diffusion characteristics as might be expected. Figures 10 and 11 show penetrative convection phenomena in which the ocean surface temperature is greater than air temperature. In such situations (Figures 10 and 11), the complex interactions of the entrainment of environmental air into the plume by its internal turbulence, and detrainment of plume matter into the atmosphere by its turbulence created difficulties in determing the boundary contours of plume and estimation of σ_y values (Table 2). In Figures 10 and 11, it is implied that the plumes have been thoroughly mixed vertically. This suggests that, at least for short periods of time, turbulence is a parameter that can be advected with mesoscale airflow.

From Figures 10 and 11, it appears that wind shear is practically always present and acts to elongate a smoke cloud and tears it apart. Often, this effect is so strong that it tends to mask the small-scale effect of diffusion. It must be emphasized, however, that wind shear and eddies due to turbulence are really indistinguishable except for their difference in scale, and it is probably impossible to draw a line of demarcation between the two. This is done in practice to simplify the analysis, and an arbitrary assumption has been made to the effect that diffusion acts to spread the smoke plume radially, while shear acts to alongate it

[Kellogg, 1956]. Actually, this means that we are eliminating from consideration the effects of those eddies that are larger than the size of the smoke cloud, and calling their effect 'shear.' The radial growth of the smoke cloud size does not depend on wind shear or wind speed but does show an increase with height (Figure 10). Figures 10 and 11 do seem to show meandering. In the atmosphere, fluctuations of a period of less than one hour are extremely important in terms of producing plume meander, which, it is felt, causes considerable oscillation of the plume about its smoothed azimuth. The effect of such higher frequency motions is to cause the plume axis not to lie along a straight line, and also to result in considerable lateral fluctuations of the location of the fumigation spot. It is not easy to treat these small scale fluctuations in a direct manner without having accurate turbulent measurements. Also, complex interactions with synoptic and convective systems produce a distressing variety of mesoscale regimes which can affect the diffusion and transport of pollutants.

5.3. Long Plumes

Smoke plumes detected by LANDSAT (Figures 6, 7, 9, 12, and 13) from the National Chemicals Industry at the Cabo Frio region are drifting more than 79 km downwind. Lyons and Pease [1973] have also summarized similar satellite observations of smoke plumes from the industries at the southern end of Lake Michigan.

In Figures 6, 7, 12, and 13, the bend in the plume axis is mostly a clockwise turning (in a coordinate system aligned with the wind). This may be more a feature of the land-sea breeze circulation than a meandering. Figure 9, on the other hand, does seem to show meandering (see discussion of short plumes). The great initial turbulence within the plumes is such that active diffusion predominates over passive for several kilometers downwind. The strong thermal stability appears more effective in damping the vertical turbulence components than the horizontal (Figures 7, 12, and 13). During more stable conditions (Figures 7, 12, and 13), the plumes were often very narrow and cohesive, staying close to the water for distance of 80 km or more, even with wind speeds on the order of 4-5 m s^{-1}. Figures 7 and 13 show that the diffusive capacity of the air into which a pollutant is emitted is limited in the vertical by a more stable layer above. This may be interpreted in terms of the concept of the well-known Reynold's stress, which says, in effect, that eddy stress is proportional to the vertical transport of momentum, and this is given by $\overline{\rho u'w'}$, where u' and w' are associated horizontal and vertical components of eddy velocity, and ρ is the air density. Clearly, the growth of the smoke cloud at first will be proportional to these eddy velocities; and, so, it may be said that the vertical transport of momentum is proportional to the mass growth; and this, in turn, should be inversely proportional to the stability of the atmosphere $(g/\bar{\theta})\ (\partial\theta/\partial z)$ (where θ is potential temperature), which will tend to suppress the vertical transport of any property. Thus, the above argument suggests why one would expect the inverse relationship between these two parameters, as displayed very markedly in Figures 7 and 13.

Figure 7 is quite typical in nature. Rows of cumulus clouds were formed a few kilometers offshore. What is relevant here is that the air mass in question has been transformed from stable (or perhaps near neutral) stratification over land to an ever deepening layer of neutral to slightly superadiabatic lapse in a relatively short distance from the shore line. At the surface, Phillips [1972] has also found that approximately 50% of the total air temperature modification takes place within the first 10 min of over water fetch. In the vertical, the air mass modification is more complex. From Table 1, it can be noticed that there was a higher level inversion on June 23, 1976. Generally, this is a synoptic subsidence inversion. In a series of aircraft measurements, Lenschow [1973] illustrated that an elevated inversion is usually present in the offshore flowing air stream. The inversion surface over the lake is usually severely altered, generally increasing with height with downwind fetch, capping a mixed layer. Lavoie's [1972] numerical model of lake effect storms shows that the inversion deformation over the lake and for many tens of kilometers inland can be a spatially complex pattern of quite significant magnitude. While for the most part the inversion base is increased to greater heights, some results suggest that it may actually decrease several hundred meters in height over the upwind shoreline regions. This is in response to the intense mesoscale divergence in the low level flow found over the upwind shoreline region. Thus, estimating mixing depths in and around, and even upwind of a Great Lakes shoreline during these lake effect storms can be more complicated than one might expect. Of course, the same phenomena occur over oceans on a much larger scale. One merely need glance at any satellite photograph taken during winter (e.g., Figure 7) to see the convective cloud lines over oceans whenever cold air streams over warmer water [Tsuchiya and Fujita, 1967].

5.4. Evaluation of Diffusion Parameters

As suggested in the introduction, the phenomenon of plume spread can be quite complex unless some simplifications can be made by careful scrutiny of the physics of the problem. Therefore, in this section, important deductions will be made from the LANDSAT imagery of smoke plumes and established physical laws of fluid mechanics. The LANDSAT images have been characterized by a gradient Richardson number (RI) computed from radiosonde and surface observations (Table 1). The RI values given in Table 1 are approximate due to the extrapolation involved in the data sets. However, on the basis of RI values, we classified the LANDSAT images into quasi-neutral cases (i.e., n = 1, 2, 3, 4, 6, 7, 9) and stable cases (i.e., n = 5, 8, 10, 11).

Measurements of the plume geometry (such as Figure 2) provide estimate of lateral standard deviation σ_y that was associated with the plume's diffusion in downwind distance (see

TABLE 3. Lateral Eddy Diffusivity Coefficient (K_y) Values Derived From Smoke Plumes of the LANDSAT Imagery

n	RI	$\bar{u}$, m s^{-1}	X_t, km	Y_m, m	$(K_y)_4$, m^2 s^{-1}	Mean $(K_y)_2$ m^2 s^{-1}	$\frac{(K_y)_2}{(K_y)_4}$
1	- 0.071	4.8	50	1118	84	64	0.76
2	- 0.065	4.6	40	1415	161	173	1.08
3	- 0.013	1.6	40	1466	60	30	0.49
4	- 0.028	6.4	120	1810	122	124	1.02
5	0.046	4.1	130	937	19	21	1.08
6	- 0.085	10.7	40	1161	252	199	0.79
7	0.006	8.0	100	2374	315	282	0.90
8	0.081	4.0	20	344	17	62	3.74
9	- 0.106	3.3	30	2335	418	70	0.17
10	0.040	5.0	80	959	40	67	1.66
11	0.088	4.6	130	727	13	19	1.48

X_t is total plume length and $Y_m = 2\ Y_0 = 4.3\ \sigma_y$ (see equation (6)). $(K_y)_4$ is obtained from (4). Mean $(K_y)_2$ is from Table 2.

section 4). The estimates of σ_y from 11 LANDSAT image cases (Figures 3–13) and calculated values of lateral eddy diffusivity coefficient (K_y) from (2) are summarized in Table 2. In every case the same corresponding 76-m height wind speed is used at different downwind distances to calculate K_y values. Mean values of σ_y and K_y for each case are given in the last column of Table 2. The values of K_y are also estimated by using the information from the LANDSAT imagery data sets in Eq. (4), and they are presented in the 6th column of Table 3 as $(K_y)_4$. Mean values of K_y from Table 2 are also presented in the 7th column of Table 3 as $(K_y)_2$. The ratio $(K_y)_2/(K_y)_4$ is included in the last column of the same table.

In Table 2, for cases n = 1, 6, and 8, we did not estimate σ_y values for long distances due to difficulty in tracing the boundaries of the smoke plumes. From Table 2 and Turner [1970], it can be seen that the estimated σ_y values over water are smaller than over land for equivalent thermal stabilities. In the previous section, we have explained the reasons for the restricted lateral spread of smoke plumes over water surfaces. The examples given are an indication of the variability of diffusion even when the overall conditions of flow appear to be in an approximately steady state. The major problem in interpretation of diffusion experiments, familiar to all works in this field, is the great variability of the observed data. In Table 2, values of K_y estimated from (2) are more consistent and they do not show any abnormal and brusque changes with downwind distance. Table 3 shows the differences in K_y from two empirical methods (i.e., Equations (2) and (4)). To determine more clearly the applicability of the two methods for estimating K_y in the Gaussian plume formula, we examined the ratio of $(K_y)_2/(K_y)_4$. The last column of Table 3 shows that the ratio $(K_y)_2/(K_y)_4$ is sufficiently close to unity in some cases. Equation (2) overestimates the values of K_y in comparison with Equation (4) in more stable conditions, whereas it underestimates in more unstable conditions.

The major difficulties encountered in the application of (5) are the correct estimation of the parameters X_m and Y_m from the LANDSAT imagery. Boundary layer turbulence is governed by the mechanical and thermal properties of the underlying surface. The relationship between mean values and vertical gradients of such properties as wind, temperature, and humidity, and surface mechanical and thermal properties was the principal subject of the presentation and discussion so far. These properties are assumed in the diffusion models, to affect the mean concentration distribution through their control of atmospheric diffusion. In the case of Gaussian diffusion models the influence of the mean concentration distribution occurs on the parameters X_m and Y_m. Of course, it is also understood that other hypothetical distributions of plume particulate density analysis could also present difficulties in choosing correct X_m and Y_m values. But the capability to determine absolute densities has not yet been validated experimentally, except in the case of lidar technique. The input parameters X_t, X_m, and Y_m would in effect create abrupt changes in K_y values. Fortunately, there is less difficulty in the determination of the total plume length (X_t) from the LANDSAT images. Equation (4) contains only one approximately estimated parameter Y_m, whereas (5) involves two parameters X_m and Y_m. Therefore, the estimated K_y values from (5) are more erratic compared to results from (4). This fact restricted the applicability of (5) to calculate K_y in the present investigation. From Tables 2 and 3, we might conclude that (2) and (4) give more realistic values for K_y. In addition, for practical purposes, (2) gives much better results than (4) if we have correct estimates of σ_y with downwind distance. The calculations indicate that the values of K_y vary from 13 to 418 m^2 s^{-1} over the Atlantic ocean. The K_y values increase in unstable conditions and they decrease rapidly in stable conditions.

The dispersion parameter σ_y^2 obtained from LANDSAT imagery is plotted in Figures 14 and 15 as a function of downwind distance from the source. In Figures 14 and 15, the straight lines estimated by eye fit the points on log-linear

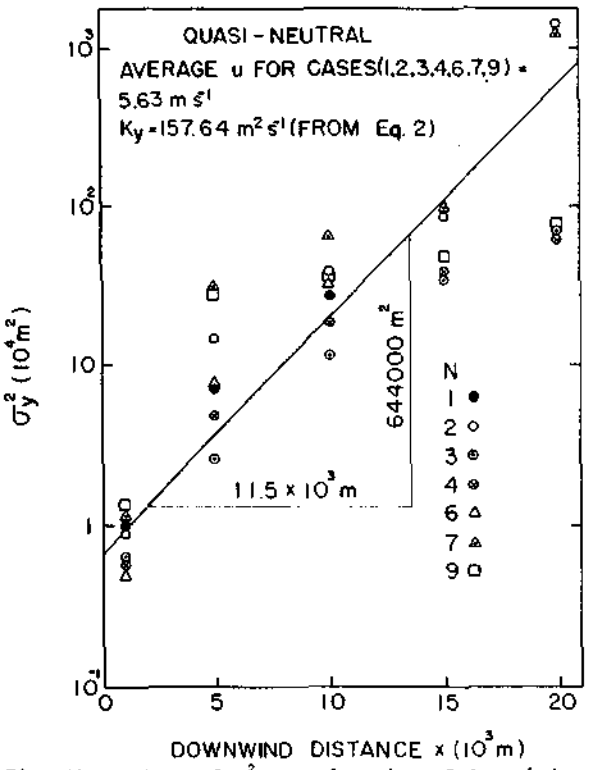

Fig. 14. Values of σ_y^2 as a function of downwind distance (x) in quasi-neutral conditions.

paper quite well. Still, there is a considerable scatter about the line. There seems to be little doubt that much of the observed variability was due to inherent properties of the field of flow, including the presence of large-scale horizontal eddy motion that produced meandering and distortion of the plume on some occasions. A part of scatter may be attributed to the technique used in estimating σ_y. It is interesting to note that the σ_y^2 values can indeed be used to calculate average lateral diffusion coefficient in quasi-neutral and stable conditions. The coefficients are then estimated to be 157.64 $m^2\ s^{-1}$ and 48.59 $m^2\ s^{-1}$ for quasi-neutral and stable stratifications, respectively, with the average wind speed being, respectively, taken as 5.63 m s^{-1} and 4.43 m s^{-1} (Figures 14 and 15).

The rate of kinetic energy dissipation ε by viscous processes can be regarded as a good indicator of the strength of turbulence. With the aid of certain approximations, the LANDSAT data sets can be used to make estimates of ε in all eleven cases. Thus, we assumed an isotropic turbulence and inertial range spectrum to estimate ε from (3). The results are shown in Table 4 together with other parameters. These values of ε show the weaker mixing processes in the marine boundary layer. The mean ε values show how sensitive the thermal inertial boundary layer can be to changes in wind, insolation, etc. They must be regarded as tentative, owing to the subjective nature of the identification of turbulence categories, and the diverse sources used in computations. There are methods to estimate ε from turbulent measurements. It is not known which estimate of energy dissipation is more reliable. The values we have obtained for ε are consistent with the values of Volkov et al. [1968], Takeuchi and Ito [1974], and Bunker [1977]. The mean values presented in Table 4 for K_y compare well with the results of Randerson et al. [1971], Takeuchi and Ito [1974], and Pond and Bryan [1976]. Lilly et al. [1974] have showed that the ε is subjected to large variations with underlying surface characteristics, height, latitude, and season. Also, the measurements over water are difficult because the spectra extend to very small scales.

There are several possible sources of error in the above computations. Acceptable errors would have been encountered in all instances in any case because of satellite position in relation to the study area, and the size of an individual grid cell in comparison with the magnitude of possible error [Ernest, 1975; Ernest and Lyons, 1974]. Some error may arise from assuming an inertial range spectrum to compute dissipation rate. Also, the vertical, lateral and longitudinal turbulence differed substantially from the assumption of isotropic turbulence. There are no direct atmospheric data against which to test these predictions.

6. Concluding Remarks

An analysis of the smoke plumes from a LANDSAT imagery of the Cabo Frio region has been described. The eleven images selected were of different months and years. These provided intimate descriptions of transport paths and dispersion processes of the smoke plumes over an ocean area. The lateral standard deviation was

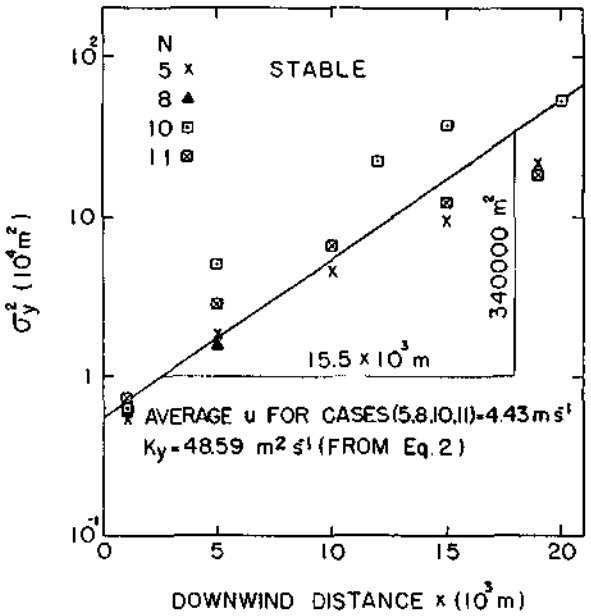

Fig. 15. As in Figure 14 except for stable conditions.

TABLE 4. Estimation of the Rate of Kinetic Energy Dissipation (ε) from Smoke Plumes of the LANDSAT Imagery

n	RI	Mean σ_y, m	Mean K_y, $m^2\ s^{-1}$	Mean ε, $m^2\ s^{-3}$ x 10^{-5}
1	- 0.071	293	64	3.4
2	- 0.065	639	173	3.1
3	- 0.013	409	30	0.1
4	- 0.028	425	124	5.9
5	0.046	238	21	0.3
6	- 0.085	313	199	80.2
7	0.006	724	282	8.2
8	0.081	241	62	7.0
9	- 0.106	570	70	0.3
10	0.040	424	67	0.9
11	0.088	250	19	0.2

Mean values of σ_y and K_y are from Table 2

selected as a measure of plume width and estimated from the plume geometry. Examination of the data sets shows that plume behavior is highly dependent on the stability of low-level air over the ocean. During the warm season, when well mixed air flows over a relatively colder water surface, intense stabilization occurs. It was to be anticipated that the existence of a strong inversion in the temperature profile at some level would decisively halt the upward spread of the particles by convection, and also that in the absence of convection, even without marked stability, the vertical spread would be very slow. This results in concentrated plumes at appreciable long distances over the ocean from the source. However, small changes in wind direction and meander of the plume disturb the plume geometry. It is somewhat uncertain, however, that the effect of meander becomes in the extremely stable flows.

With two empirical methods, the K_y values were evaluated from plume dimensions. Calculations of K_y yielded values ranging from 13 to 418 $m^2\ s^{-1}$ in quasi-neutral and stable conditions. A K_y value of about 157.64 $m^2\ s^{-1}$ in quasi-neutral and 48.59 $m^2\ s^{-1}$ in stable conditions were obtained from a plot of σ_y^2 as a function of distance from the source. Most consistent estimates for K_y were obtained from (2). The values of ε have been estimated over water from σ_y and K_y values. These results compare very well with previous experimental results over water surfaces.

The data described in the present study are isolated examples from which only tentative and rather qualitative deductions are made. Much more data would be required to establish a relation, but this first indication is at least a pointer to the practical analysis of horizontal diffusion. Because of logistic and financial constraints only data from the LANDSAT system were examined. With an observation frequency of once per 18 days, the data sample is likely to be small indeed. Unfortunately, in many impact statements, owing to pressures which are entirely understandable, data from the nearest national weather service office are used in preparing calculations. Thus, the most critical conditions might often be missed. There are probably more important differences in mesoscale climate in the 200 km east of the Cabo Frio region.

Unfortunately, the various aspects of the problem are so diverse that a good synthesis is not yet possible. Yet it was felt that in the long run, it would be beneficial to delve into some of the details surrounding the various case studies. We will present in future publications our studies of the simplest case, diffusion over water, complicated only by the fact of varying water surface temperatures or the intense modification which occurs when air crosses the shoreline to traverse water of differing temperature. We will also discuss the basis of mesometeorological systems over water inasmuch as diffusion (and transport) in intimately intermingled with atmospheric behavior on the mesoscale.

The atmosphere is not an infinite simply-connected domain, and this, combined with its rotation, must force a state of non-homogeneity, even in the horizontal, on the largest scale. Other limitations of the present treatments will occur to the meteorological reader, but we would prefer to close on a hopeful note in remarking on the progress made towards our needs by the extension to anisotropy and to a turbulent field assumed to exist without mean motion.

Acknowledgements. The authors are thakful to Nelson de Jesus Parada, director, and Antonio Divino Moura, chief of the Department of Meteorology, Instituto de Pesquisas Espaciais, São José dos Campos, São Paulo, Brazil, for their encouragement. They would like to acknowledge the assistance of José Carlos Moreira in the LANDSAT imagery analysis. Thanks are due to Renato Herz for reading the manuscript, Carlos Roberto dos Santos and his group members for drafting the figures and Célia Regina Rosa for typing the manuscript. This work was partially supported by the Financiadora de Estudos e Projetos (FINEP) under contract B/54/81/042/00/00.

References

Batchelor, G. K., Diffusion in a field of homogeneous turbulence, 1, Eulerian analysis, Aust. J. Sci. Res., 2, 437-450, 1949.

Batchelor, G. K., Diffusion in a field of homogeneous turbulence, 2, The relative motion of particles, Proc. Cambridge Philos. Soc., 48, 345-362, 1952.

Browne, N. E., Some measurements of diffusion parameters from smoke plumes, Bull. Am. Meteorol. Soc., 42, 101-105, 1961.

Bunker, A. F., Structure, turbulence, fluxes, and transformations of a maritime cold front during AMTEX, J. Meteorol. Soc. Jpn., 55, 586-604, 1977.

Csanady, G. T., Diffusion in an Ekman layer, J. Atmos. Sci., 26, 414-426, 1969.

Csanady, G. T., Crosswind shear effects on atmospheric diffusion, Atmos. Environ., 6, 221-232, 1972.

Culkowski, W. M., Time exposure photography of smoke plume, USAEC Rep. ORO-359, Weather Bureau, Oak Ridge, Tenn., 1961.
Ernest, J.A., New synchronous meteorological satellite, SMS-2, Weatherwise, 28, 151-177, 1975.
Ernest, J. A., and W. A. Lyons, Inadvertent weather modification by Chicago-Northern Indiana pollution sources observed by ERTS-1, Mon. Weather Rev., 102, 503-508, 1974.
Frenkiel, F. N., and I. Katz, Studies of small--scale turbulent diffusion in the atmosphere, J. Meteorol., 13, 388-394, 1956.
Força Aérea Brasileira, Upper Air data of January 1974 to December 1978 at the international airport of Galeão, Rio de Janeiro, Brazil, Força Aérea Brasileira, 1974-1978.
General Electric Company, IMAGE 100 interactive multispectral image analysis system-technical proposal, Proposal 717001, Ground Systems Department Space Division, General Electric Company, Daytona Beach, Fl., 1974.
General Electric Company, IMAGE 100 User manual, Ground Systems Department Space Division, General Electric Company, Daytona Beach, Fl., 1975.
Gifford, F., Relative atmospheric diffusion of smoke puffs, J. Meteorol., 14, 410-414, 1957.
Gifford, F., Smoke plumes as quantitative air pollution indices, Int. J. Air Pollut., 2, 42-50, 1959.
Gifford, F., Uses of routine meteorological observations for estimating atmospheric dispersion, Nucl. Saf., 2, 47-51, 1961.
Gifford, F., An outline of theories of diffusion in the lower layer of the atmosphere, in Meteorology and Atomic Energy, edited by D. H. Slade, pp. 65-116, U.S. Atomic Energy Commission, National Technical Information Service, Springfield, Va., 1968.
Griggs, M., Determination of aerosol constant of the atmosphere, in Symposium on Significant Results Obtained From the Earth Resources Technology Satellite, NASA Goddard Space Flight Center, Greenbelt, Md., 1973.
Heisenberg, W., Zur statistischen theorie der turbulenz, Z. Physik, 124, 628-657, 1948a.
Heisenberg, W., On the theory of statistical and isotropic turbulence, Proc. R. Soc. London Ser. A, 195, 402-406, 1948b.
Högström, U., An experimental study of atmospheric diffusion, Tellus, 16, 205-251, 1964.
Holland, J. Z., A meteorological survey of the Oak Ridge area: Final report covering the period 1948-1952, USAEC Rep. ORO-99, Weather Bureau, Oak Ridge Tenn., 1953.
Instituto Nacional de Meteorologia, Meteorological data of 1968 to 1978 from the station, Fabrica Nacional de Alcalis, Cabo Frio, Instituto Nacional de Meteorologia, Brazil, 1968-1978.
Kellogg, W. W., Diffusion of smoke in the stratosphere, J. Meteorol., 13, 241.250, 1956.
Lavoie, R. L., A mesoscale numerical model of lake effect storms, J. Atmos. Sci., 29, 1025-1040, 1972.
LeMone, M. A., Workshop on the Planetary Boundary Layer, pp. 182-246, American Meteorological Society, Boston, Mass., 1980.
Lenschow, D. H., Two examples of planetary boundary layer modification over the Great Lakes, J. Atmos. Sci., 30, 568-581, 1973.
Lilly, D. K., D. E. Waco, and S. I. Adelfang, Stratospheric mixing estimated from high--altitude turbulence measurements, J. Appl. Meteorol., 13, 488-493, 1974.
Lyons, W. A., Satellite detection of air pollutants, in Remote Sensing Energy-Related Studies, edited by T. N. Vaziroglu, pp. 263--290, John Wiley, New York, 1975a.
Lyons, W. A., Turbulent diffusion and pollutant transport in shoreline environment. in Lectures on Air Pollution and Environmental Impact Analysis, pp. 136-208, American Meteorological Society, Boston, Mass., 1975b.
Lyons, W. A., and S. R. Pease, Detection of particulate air pollution plumes from major-point sources using ERTS-imagery, Bull. Am. Meteorol. Soc., 54, 1163-1170, 1973.
McLellan, A., Satellite remote sensing of large scale local atmospheric pollution, paper presented at the International Clear Air Congress, Air Pollution Control Assoc., Pittsburgh, Pa., 1971.
Mekler, Y., H. Quenzel, G. Ohring, and I. Marcels, Relative atmospheric aerosol content from ERTS observations, J. Geophys. Res., 82, 967-970, 1977.
Nicolli, D., Altura da camada de inversão térmica e potencial de poluição do ar, Relatório DR/GAL(MTL)-001-77, Comissão Nacional de Energia Nuclear, Brazil, 38 pp, (in Portuguese), 1977.
Pasquill, F., The estimate of the dispersion of windborne material; Meteorol. Mag., 90, 33-46, 1961.
Phillips, D. W., Modification of surface air over Lake Ontario in winter, Mon. Weather Rev., 100, 662-670, 1972.
Pond, S., and K. Bryan, Numerical models of the ocean circulation, Rev. Geophys. Space Phys., 14, 243-253, 1976.
Prophet, D. T., Survey of the available information pertaining to the transport and diffusion of airbone material over ocean and shoreline complexes, Tech. Rep. 89, 53 pp., Aerosol Lab., Stanford Univ., Stanford, Calif., 1961.
Randerson, D., A study of air pollution sources as viewed by earth satellite, J. Air Pollution Control Assoc., 18, 249-253, 1968.
Randerson, D., J. G. Garcia and V. S. Whitehead, Photogrammetric and Photometric investigation of a smoke plume viewed from space, J. Appl. Meteorol., 10, 1122-1131, 1971.
Raynor, G. S., P. Michael, R. M. Brown, and S. SethuRaman, Studies of atmospheric diffusion from a nearshore ocean site, J. Appl. Meteorol., 14, 1080-1094, 1975.
Raynor, G. S., R. M. Brown, and S. SethuRaman, A comparison of diffusion from a small island and a undisturbed ocean site, J. Appl. Meteorol., 17, 129-139, 1978.
Richardson, L. F., Some measurements of atmospheric turbulence, Phil. Trans. R. Soc. London, Ser. A, 221, 1-28, 1920.
Richardson, L. F., Atmospheric diffusion shown on a distance neighbour graph, Proc. R. Soc. London, Ser. A, 110, 709-737, 1926.
Roberts, O. F. T., The theoretical scattering of smoke in a turbulent atmosphere, Proc. R. Soc. London, Ser. A, 104, 640-654, 1923.

Saffman, P. G., The effect of wind shear on horizontal spread from an instantaneous ground source, Q. J. R. Meteorol. Soc., 88, 382-393, 1962.

Silva, P. C. M., Upwelling and its biological effects in Southern Brazil, in Fertility of the Sea-2, edited by J. D. Costlow, Jr., pp. 469-474, Gordon and Breach, New York, 1971.

Slade, D. H., Atmospheric dispersion over Chesapeake Bay, Mon. Weather Rev., 90, 217-224, 1962.

Smith, F. B., The role of wind shear in horizontal diffusion of ambient particles, Q. J. R. Meteorol. Soc., 91, 318-329, 1965.

Sutton, O. G., A theory of eddy diffusion in the atmosphere, Proc. R. Soc. London, Ser. A, 135, 143-165, 1932.

Takeuchi, K., and S. Ito, Estimation of the diffusion coefficient of thermal pollution, Adv. Geophys., 16A, 384-390, 1974.

Taylor, G. I., Diffusion by continuous moments, Proc. London Math. Soc., 2, 196-211, 1921.

Tsuchiya, K., and T. T. Fujita, A satellite meteorological study of evaporation and cloud formation over the western Pacific under the influence of the winter monsoon, J. Meteorol. Soc. Jpn., 45, 232-250, 1967.

Turner, D. B., Workbook of Atmospheric Dispersion Estimates, 84 pp., Environmental Protection Agency, Office of Air Programs Research Triangle Park, North Carolina, 1970.

Tyldesley, I. B., and C. E. Wallington, The effect of wind shear and vertical diffusion on horizontal dispersion. Q. J. R. Meteorol. Soc., 91, 158-174, 1965.

Van der Hoven, I., Atmospheric transport and diffusion at coastal sites, Nucl. Saf., 8, 409-499, 1967.

Volkov, Yu, A., V. P. Kukharets, and L. R. Tsvang, Turbulence in the atmospheric boundary layer above steppe and sea surface, Izv. Atmos. Ocean. Phys., 4, 591-599, 1968.

Whitehead, V. S., I. D. Browne, and J. G. Garcia, Cloud height contouring from Apollo 6 photography, Bull. Am. Meteorol. Soc., 50, 522-528, 1969.

World Meteorological Organization, Climatic Atlas of South America, Unesco, Budapest, Hungary, 1975.

(Received December 23, 1981;
revised April 19, 1982;
accepted May 19, 1982.)